

# Unravelling Tool Edge Trajectory Patterns: Implications on Surface Roughness in End Milling Process

*Fatiha Naziera Yusof, Mohd Fauzi Ismail\**

*School of Mechanical Engineering, College of Engineering,  
Universiti Teknologi MARA, 40450 Shah Alam, Selangor, MALAYSIA*

*\*mohdfauzi305@uitm.edu.my*

*Rizal Mohamed Noor*

*School of Mechanical Engineering, Universiti Teknologi MARA,  
Pulau Pinang Branch, Permatang Pauh Campus, Pulau Pinang, MALAYSIA*

## ABSTRACT

*This study examines the effect of end milling on surface roughness in modern manufacturing. Mathematical equations simulate and analyse the tool edge trajectory of a two-flute end mill during end milling. The results are refined using MATLAB and watershed segmentation. An aluminium alloy flat bar is end-milled using a CNC milling machine for the experimental phase. Optical 3D surface measurements provide roughness data for analysis. The study shows that higher spindle speeds produce smoother surfaces with improved surface quality. The correlation matrix analysis highlights the significance of spindle speed in shaping surface roughness, and tool trajectories are associated with softer surfaces at elevated speeds for the spindle speed ranging between 1000 to 3500 rpm. The study offers valuable insights into the complex relationship between tool edge trajectories and surface roughness.*

**Keywords:** *Machining Processes; End Milling; Surface Roughness; Tool Edge Trajectory; CNC Milling*

## Introduction

Machining processes are always in high demand in the aerospace, automotive, medical, and naval industries. Since the beginning of the industrial era, machining processes have played a fundamental role in

shaping modern manufacturing, enabling the production of parts with precise surface quality and geometric accuracy. Conventional machining, in combination with computer numerical control (CNC), enhances versatility and increases the dependency of many industries on the technology [1].

At the heart of machining techniques, milling is a prominent cutting procedure. It involves primary motion generated by the rotation of the milling head and auxiliary motion driven by the workpiece moving perpendicular to the cutter axis, an essential feature for creating complex parts. End milling stands out and is acclaimed for efficient material removal with maintained surface quality, enabling diverse configurations using milling cutters [2].

Over several decades, a substantial body of theoretical and experimental research has been dedicated to understanding machined products' surface profiles and roughness. Experimental approaches, including those involving Artificial Neural Networks (ANN) [3]-[5], Design of Experiment (DoE) [6], Response Surface Method (RSM) [7]-[8], gene expression programming method [9], and linear regression analysis [10], aim to correlate machining parameters with surface roughness parameters such as  $Ra$  (arithmetical mean of the absolute surface heights). However, these approaches often do not consider the physical aspects of the tool-work interaction during the formation of surface texture.

The geometrical transfer from the tool to the work surface is one of the many factors contributing to creating the work surface texture and, consequently, its surface roughness. Ideally, this geometrical transfer creates the work surface texture and affects surface roughness. The work surface condition becomes predictable when the tool has a known perfect shape.

Simulation is a computational method used to create models that simulate the formation of the machined surface profile, enabling the visualisation and evaluation of surface texture and roughness [11]. Simulation allows observing potential outcomes, reducing expensive experimental work's material and effort requirements. While it cannot guarantee precise results, it approximates actual outcomes. Simulation has a long history in machining, and its use in predicting surface roughness has yielded remarkable results. Several research reports focus on 3D surface topography modelling for the geometrical transcription of the tool during face milling [12]-[13] and ball-end milling [14]-[16]. Most of this research focuses on tools with prominent geometric characteristics of tool cutting tips; none addresses the flat-end milling tool.

This research's primary objective is to comprehensively analyse a two-flute end mill's tool edge trajectory pattern during end milling processes. This study introduces a mathematical model to simulate the trajectory of a tool's edge as it interacts with the workpiece surface during end milling. This is achieved by developing a mathematical model and investigating the impact of varying spindle speeds on both simulated and experimental surface lay

patterns. Furthermore, the study aims to establish a connection between these surface lay patterns and workpiece roughness parameters.

## **Methodology**

### **Simulation process**

The study employs a systematic simulation process meticulously designed to predict and analyse the intricate tool edge trajectory pattern generated by two-flute end mills during the end milling process, providing valuable insights into surface roughness. The simulation process consists of four stages as follows.

### Governing equation

The initial stage revolves around formulating a foundational mathematical equation that precisely captures the complex trajectory of the end mill cutting tool edges during end milling. This equation harmoniously integrates critical variables encompassing the cutting tool's radius ( $R$ ), spindle speed ( $W$ ), and feed rate ( $f$ ). Derived from Equation (1) and Equation (2), this equation is the foundation for the following stages, offering a dependable representation of the tool's path on the machined surface. Equation (1) estimates the location of the tool edge of the first flute on the x-y plane, while Equation (2) estimates the position of the tool edge of the second flute at the time  $t$  for a 2-flute end mill cutting tool.

$$\begin{aligned}x(t) &= -R \cos(2W\pi t) + (ft) \\y(t) &= R \sin(2W\pi t)\end{aligned}\tag{1}$$

$$\begin{aligned}x(t) &= -R \cos(2W\pi t - \pi) + (ft) \\y(t) &= R \sin(2W\pi t - \pi)\end{aligned}\tag{2}$$

### Tool edge trajectory plot

This research prepares graphs or plots depicting the tool edge trajectory of a 2-flute end mill under various machining conditions. MATLAB R2017 is utilised to transform these plots into grayscale images, and a meticulous calibration process ensues to ensure accurate alignment and scaling. This careful calibration accurately depicts the tool's movement across the machined surface. A grayscale image processing approach compares these image plots with surface topography characterised by hills and valleys. This study applies a similar approach to the tool edge trajectory plots, where darker trajectory lines signify valleys, while the brighter background represents hills. Subsequently, the plot images are resized to a consistent area dimension and converted into grayscale surfaces, where the z-axis corresponds to the grayscale values. To ensure precise characterisation and

quantification, the x and y axes of these grayscale images/surfaces depicting the tool's trajectory are correctly calibrated. The cropping of the plots is achieved by utilising a specialised algorithm known as SurfSuite, which is part of a Surface Analysis System. It is important to note that SurfSuite is a specialised MATLAB tool developed with a user-friendly Graphical User Interface (GUI) tailored to enhance the precision and reliability of the simulation tasks at hand.

### Extracting pattern fragments

The tool edge trajectory of the 2-flute end mill tool in some time  $t$  results in fragmented patterns with the trajectory curves as the boundaries. Watershed segmentation in MATLAB R2017 is employed to partition the grayscale image of the tool edge trajectory plot and isolate each fragmented pattern into distinct regions or segments with the trajectory curves as their boundaries, thereby providing detailed information about each segment, including its size measured in pixel units. Each segment is uniquely color-coded to represent its surface area. When analysing the tool edge trajectory pattern, variations in curvature and intersections result in segments of varying sizes. Varying spindle speeds ( $W$ ) under different cutting conditions leads to discrepancies in the number and size of these segmented areas. This study's primary focus is on the analysis of these segmented areas. For each surface or cutting condition, various statistical metrics related to the segmented regions, such as the count of segmented regions, standard deviation, and average size, are utilised to characterise the trajectory pattern. These statistical measures help identify and analyse the differences between different sets of machining conditions.

### Quantification

In the final stage, the segmented plot is subjected to quantification and statistical analysis. This step uses Microsoft Excel 2019 to extract statistical quantity from the segmented plot. Parameters of interest include the number and area size of segments.

### **Transition to experimental phase: application and measurement**

The machining process involves using the DMG MORI DMU 50, a 5-axis universal CNC milling machine, to mill flat bars made of aluminium alloy, specifically the 6061 alloy, based on the parameters detailed in Table 1. Utilising a 12 mm TiAlN-coated HRC48 carbide endmill, the samples undergo systematic machining along a designated cutting path, encompassing spindle speeds ranging from 1000 rpm to 4000 rpm. Table 2 provides a comprehensive overview of the cutting tool, including detailed specifications and characteristics. The experimental work unfolds in two distinct stages: fabrication and surface roughness measurement.

**Fabrication**

The flat bars used in the study have specific dimensions, measuring 152.4 x 88.9 x 12.7 mm, as shown in Figure 1. The initial stage involves setting up the CNC milling machine, developing a program using computer-aided manufacturing (CAM) software, and executing the milling process under the defined parameters. Two specimens are prepared, each subjected to varying spindle speed ranges. To minimise the presence of burrs, the machining process is repeated thrice for each speed range. A total of 7 distinct end milling patterns are meticulously produced, with the feed rate remaining constant at 2000 mm/min to ensure a consistent travel length of 88.9 mm. Tables 3 and 4 provide detailed information on the workpiece's chemical, mechanical, and physical properties.

Table 1: End milling parameters for the experimental phase

Parameters	Samples						
	1	2	3	4	5	6	7
Spindle speed (x1000 rpm)	1.0	1.5	2	2.5	3.0	3.5	4.0
Feed rate (mm/min)	2000						
Depth of cut (mm)	0.2						
Tool path strategy	A unidirectional linear cutting trajectory						
Machining tool	A 12 mm diameter two-flute cutting tool						

Table 2: HRC48 carbide end mill specifications and end milling parameters

HRC48 carbide end mill	
Number of flutes	2
Helical	Helix 35 degree
Diameter	12 mm
Cutting length	30 mm
Length	75 mm

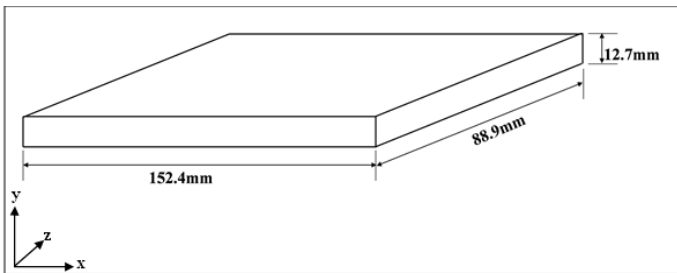


Figure 1: Schematic diagram of the workpiece

Surface roughness measurement

An optical 3D surface measurement device, Alicona Infinite Focus Microscope (IFM), is employed to capture the micro-surface topography of the milled surface. Operating on the principles of focus variation, the IFM scans surfaces at a magnification of 50x, incorporating 3x2 image stitching to obtain the morphological surface encompassing an area of 7801.02 x 3904.02  $\mu\text{m}$ .

Table 3: Chemical properties of Aluminium alloy flat bar 6061

Si	Fe	Cu	Mn	Mg	Cr	Zn	Ti	Others	
								Each	Total
0.04		0.15		0.8	0.04				
-	0.70	-	0.15	-	-	0.25	0.15	0.05	0.15
0.08		0.04		1.2	0.35				

Table 4: Mechanical properties of Aluminium alloy flat bar 6061

Property	Value
Ultimate Tensile Strength (ksi)	42
Tensile Yield Strength (ksi)	35
Brinell Hardness (500 kg load/10 mm ball)	95
Elongation % in 2 inch (1/16 in)	10
Coefficient of linear expansion (0 – 100 °C <sup>-1</sup> x 10 <sup>6</sup> )	23.6
Melting range (°C)	575 - 650
Thermal conductivity (0 - 100 °C) W/m°C	167
Electrical resistivity at 20 °C $\mu\Omega\text{cm}$	4.0

Data preprocessing and quantification

The morphological surface undergoes Gaussian bandpass filter-based data preprocessing to reduce the effect of noise in the high-frequency region and form errors in the low-frequency region. Areal surface roughness parameters are computed from the pre-processed morphological surface for quantification. The range of surface roughness parameters used is based on ISO 25178: Geometrical Product Specifications (GPS) – Surface texture: areal. The root mean square of surface amplitudes (*Sq*) and the maximum surface height (*Sz*) are amplitude parameters that measure the height standard deviation and the maximum peak-to-valley height of the surface, respectively. The developed interfacial area ratio (*Sdr*) is part of the hybrid parameters category and measures the wrinkled surface area size ratio to the flat measuring area size. The texture aspect ratio (*Str*) and the autocorrelation length (*Sal*) belong to the spatial parameter category and measure the texture pattern's symmetry and the texture dominant wavelength, respectively.

## Results and Discussion

The similarity between the end milling pattern produced by the physical end milling process Figure 3 and the simulated tool edge trajectories pattern Figure 2 is evident. The obtained end mill cutting pattern is influenced by tool engagement, workpiece interaction, and feed direction during cutting operations, aligning with prior studies by Lazoglu et al. [15] and Hadad et al. [17]. Predicted and experimental patterns showcase continuous circular patterns progressing in unison. A closer examination reveals these circular shapes touching and intersecting, resulting in two distinct forms at the centre and edges. The central shape assumes a curvilinear appearance, while the patterns at the edges resemble diamonds. This overlap of cutting marks gives rise to a boundary, forming a segment where the tool edge coincides.

However, a close examination of the pattern on the experiment surface reveals missing trajectory loops, making a gap in every other loop. As shown in Figure 3, only two large blue lobes appear at the path axis ( $y = 2000$ ), while in the simulation in Figure 2 ( $y = 6 \times 10^4$ ), the lobes are continuous without a gap, and the number is doubled for the same length on the feed direction. This is suspected due to dimensional differences of the cutting edge from the 2-flutes milling tool. This caused the difference in tool-work interaction, leaving prominent cutting marks from only one flute.

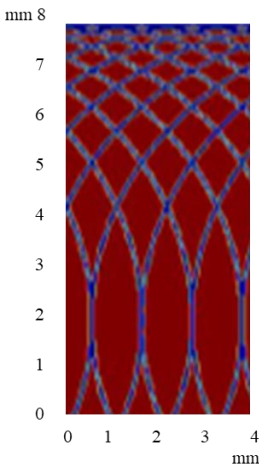


Figure 2: A representation of the tool edge trajectory pattern in the simulation

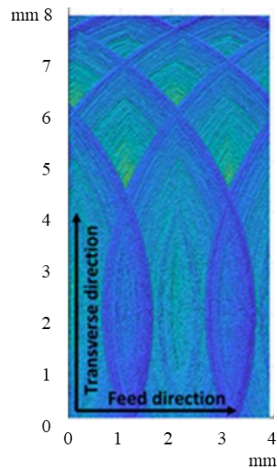

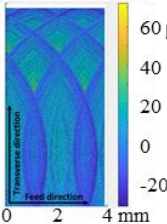
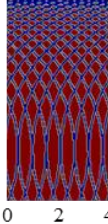
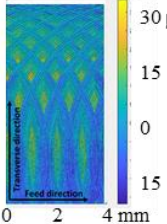
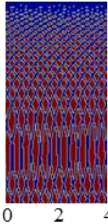
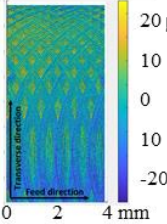
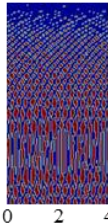
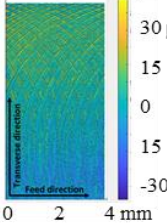


Figure 3: A depiction of the tool edge trajectory pattern through experimental optical observation

The simulation's tool edge trajectory pattern indicates that as spindle speed escalates, the segment size shrinks. The end milling pattern extracted

from practical experiments reflects a similar trend, demonstrating a decrease in segment size with increased spindle speed. This can be seen in Table 5. This is notably visible in the central zone, where the width of the curve-like pattern reduces and gives way to more curve-like shapes, known as loops.

Table 5: Segment spacing trends in cutting-edge trajectory patterns

Spindle speed (rpm)	Tool edge trajectory pattern preceding segmentation	Morphological surface by Alicona Infinite Focus Microscope (IFM)
1000		
2000		
3000		
4000		



Spindle speed impacts the number of loops in both simulated tool cutting-edge trajectories and end milling patterns. Extracted feature parameters are visually presented through graphs for clarity, and their relationships are detailed in Table 6. The focus is on the feature area due to its reliability, employing statistical measures like mean and standard deviation to represent the simulated surfaces accurately.

A notable positive correlation exists between segmented area count and spindle speed, as the trend is shown in Figure 4. Higher spindle speeds correspond to the increased segmented areas. Shifting to mean values and spindle speed correlation, a distinct negative relationship emerges. Higher spindle speeds lead to lower means, while lower spindle speeds result in higher means. Figure 4 visually depicts this pattern, showcasing a nonlinear trajectory that asymptotically tends to zero at higher spindle speeds, 3000 to 4000 rpm. Similarly, standard deviation and spindle speed correlation trend negatively. Increased spindle speed corresponds to reduced standard deviation and vice versa. Figure 5 illustrates this pattern, echoing the mean correlation but with a smoother curve and an asymptote approaching zero at higher spindle speeds. A similar trend was also observed for the mean segmented area (Figure 6). This suggests that higher spindle speeds can lead to a more uniform surface pattern and less deviated surface topography, expected to lead to finer and even surface roughness. However, there is also likely to be a threshold or saturation point on the spindle speed where the surface roughness cannot be further improved.

Table 6: Correlations among spindle speed and number, mean, and standard deviation of segmented areas in trajectory analysis

	Spindle speed	Number	Mean	Standard deviation
Spindle speed	1			
Number	0.998	1		
Mean	-0.856	-0.828	1	
Standard deviation	-0.794	-0.761	0.993	1

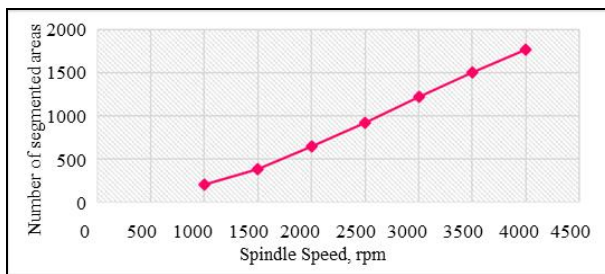


Figure 4: The influence of spindle speed on the number of segmented regions

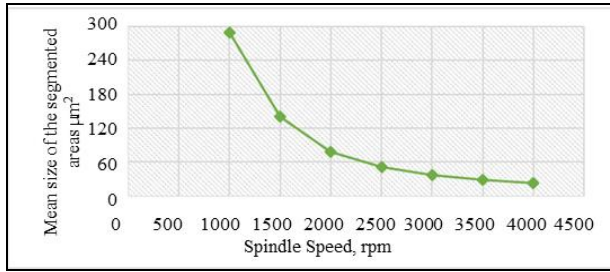


Figure 5: The influence of spindle speed on the mean of segmented areas

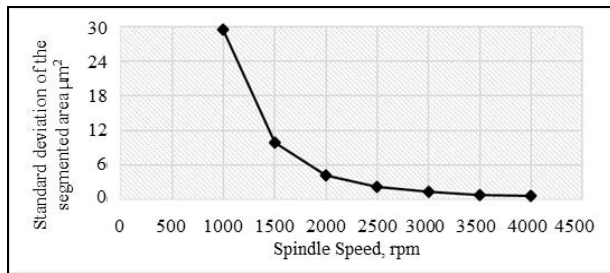


Figure 6: The influence of spindle speed on the standard deviation of segmented areas

### Analysis of experimental tool edge trajectory pattern

In evaluating the experimental tool edge trajectory pattern, this section focuses on the approach employed for measuring surface roughness. The process involves conducting an actual end milling process and utilising a three-dimensional (3D) areal surface roughness measurement method to gauge the resultant surface's roughness. This applies an optical 3D metrology system for measuring three-dimensional texture and geometrical data. This enables an automated quantification of the surface's three-dimensional attributes, enhancing the accuracy and depth of analysis.

Figure 7 provides a glimpse into the surface topography of the measured dataset for the chosen area at 1000 rpm of the experimental end mill tool edge trajectory pattern. The depiction uses accurate or pseudo-colour coding based on height. Following this, a sampling process is engaged to refine the quality of the acquired surface topography, enabling more effective analysis. Figure 8 is a filtered dataset that further refines the surface topography of the selected dataset area at 1000 rpm. This step enhances the data quality by reducing noise and errors, which can significantly impact subsequent roughness measurements. However, it is noteworthy that using a low magnification lens to capture a larger measuring area during

preprocessing can inadvertently introduce noise and errors, thereby influencing roughness measurements.

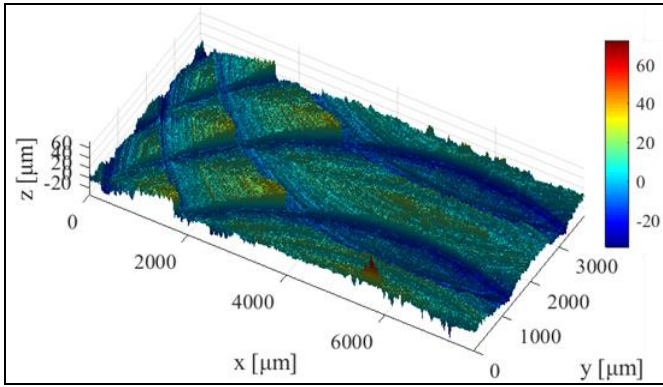


Figure 7: Pre-processed 1000 rpm area's initial surface data

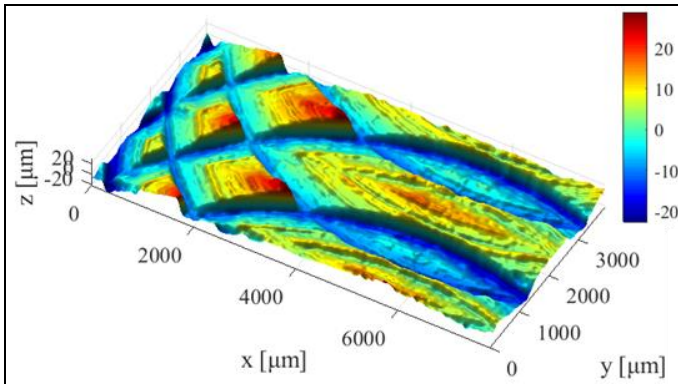


Figure 8: Preprocessing of selected 1000 rpm surface dataset area

### Surface roughness analysis and graphical correlations

This section delves into the outcomes of the surface roughness measurement of the experimental tool edge trajectory pattern. These results are reflected in Table 7.

Similar negative trends with asymptotes at higher spindle speeds are observed in Figure 9 and Figure 10 for  $Sq$  and  $Sz$ , respectively, when plotted against the spindle speed. This indicates that higher spindle speed reduces the roughness amplitude, with the threshold around 3500 rpm. Figure 11 shows that the interfacial developed area ratio  $Sdr$  also exhibits a downward trend with increasing spindle speed, with an earlier slope reduction than  $Sq$  or  $Sz$ .

Meanwhile, in Figure 12, the texture aspect ratio ( $Str$ ) maintains a relatively constant value for all spindle speeds, hovering around 0.2 to 0.3. This suggests the surfaces are isotropic, lacking a significant texture direction, as seen in the actual surface or the simulated trajectory pattern. The autocorrelation length ( $Sal$ ) also experiences a similar downward trend as  $Sq$  and  $Sz$ , with the asymptote at the higher spindle speeds (refer to Figure 13).

Table 7: Measurement data for spindle speed and four machining parameters

Spindle speed, rpm	$Sq$	$Sz, \mu\text{m}$	$Sdr$	$Str, \mu\text{m}$	$Sal$
1000	8.68	51.38	0.263	0.273	328.48
1500	7.38	41.78	0.191	0.182	279.76
2000	5.10	33.48	0.130	0.174	210.29
2500	3.95	31.83	0.110	0.268	167.14
3000	2.97	23.41	0.097	0.250	147.10
3500	2.17	18.31	0.075	0.280	139.21
4000	2.12	21.79	0.080	0.286	137.89

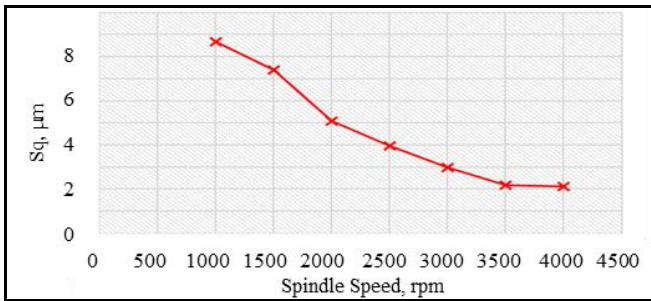


Figure 9: Influence of spindle speed on root mean square height ( $Sq$ )

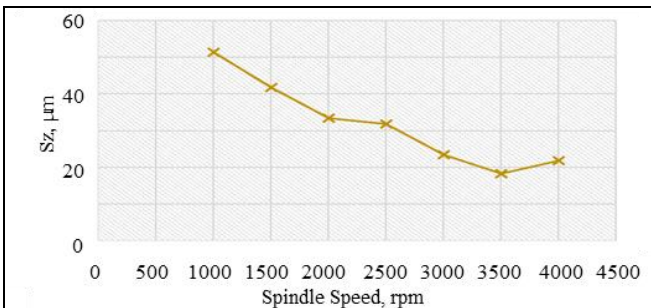


Figure 10: Influence of spindle speed on maximum surface height ( $Sz$ )

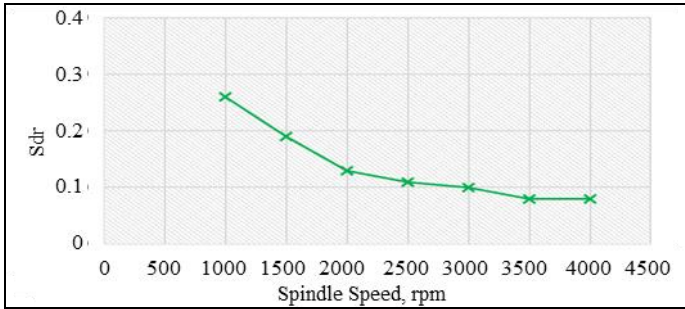


Figure 11: Influence of spindle speed on the developed interfacial area ratio ( $Sdr$ )

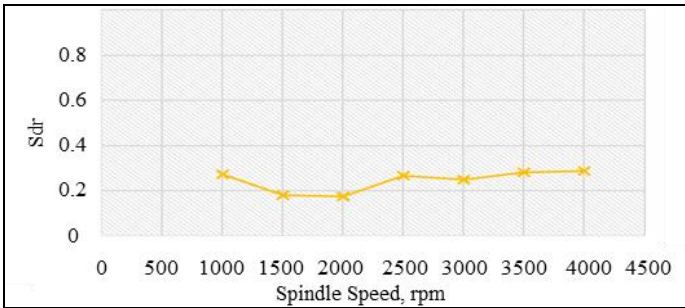


Figure 12: Influence of spindle speed on the texture aspect ratio ( $Str$ )

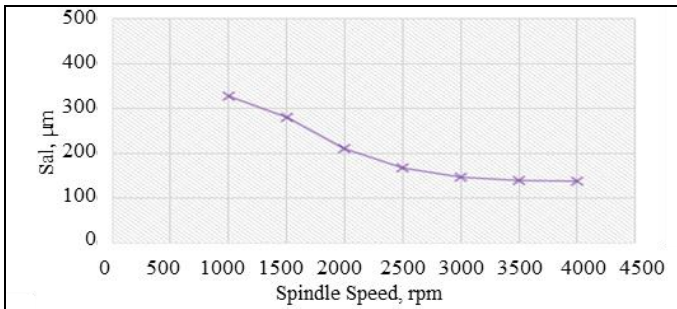


Figure 13: Influence of spindle speed on the auto-correlation length ( $Sal$ )

The trends in the graphs for roughness parameters are compared with the physical theory of tool geometric transcription. Figure 14 depicts the basic geometry of the 2-flute milling tool, while Figure 15 illustrates the surface geometry after transcription at both slow and high spindle speeds.

The similarity in the downward trend of  $Sq$  and  $Sz$  is expected, as they represent the same height parameters, while the surface textures in this study are repetitive and stable. The downtrend of  $Sq$  is similar to the trend of  $Ra$  (arithmetical mean of the absolute surface heights) documented in other experimental methods that use Artificial Neural Networks (ANN) [3]-[5], Design of Experiment (DoE) [6], Response Surface Method (RSM) [7]-[8], gene expression programming method [9], and linear regression analysis [10].  $Ra$  (arithmetical mean of the absolute surface heights) is from the profile method. In contrast,  $Sq$  (root mean square value of surface amplitudes) is from the areal method. However,  $Ra$  and  $Sq$  describe very similar properties on the amplitude of surface irregularities. The downward trend of  $Sq$  can be explained by the geometrical transcription resulting from the tool-work interaction (see Figure 14 and Figure 15).

Assuming that the 2-flute flat-end tool has a slight relief angle, as shown in Figure 14, the geometrical transcription at lower spindle rotational speeds creates a surface profile, as depicted in Figure 15a. By increasing the spindle rotational speed alone, the surface profile transforms into the configuration shown in Figure 15b, where the smaller pattern contributes to the lower  $Sq$  and  $Sz$ . Another interesting observation is that the downward trend of  $Sq$  and  $Sz$  becomes weaker at higher spindle speeds, around 3500 to 4000 rpm, corresponding to the mean of the segmented area of the simulated trajectory pattern (Figure 5). An asymptote at higher spindle speeds indicates that further improvement in work surface roughness cannot be achieved solely by increasing spindle speed, as roughness caused by factors other than simple tool geometrical transcription becomes more prominent.

The phenomenon of  $Sal$  in Figure 13 can also be explained by Figure 15, where lower spindle speed produces a more extensive surface wavelength or distance between the surface features, as seen in Figure 15a, while higher spindle speed results in a shorter surface wavelength, as shown in Figure 15b. However, increasing the spindle speed beyond 3500 rpm may not further smooth the surface roughness, as other factors besides simple tool geometrical transcription become more prominent.

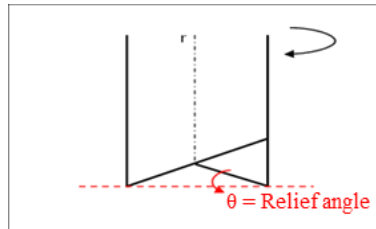


Figure 14: Tool geometry schematic diagram

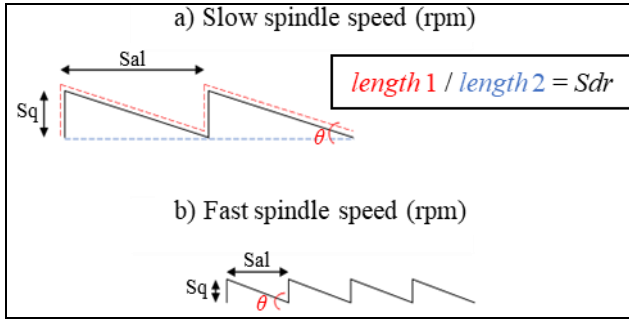


Figure 15: Surface geometry schematic diagram

On the other hand, the developed interfacial area ratio ( $Sdr$ ), as shown in Figure 11, exhibits an unexpected trend that cannot be theoretically explained based on Figures 15a and b. According to Figure 15, the ratio, developed as the sum length of triangle sides to the length of the triangle base, similar to the  $Sdr$  value, should remain constant from lower spindle speed (Figure 15a) to higher spindle speed (Figure 15b). However, the experimental results show a downward trend with increasing spindle speed. The decreasing trend of  $Sdr$  is suspected to be due to the dataset filtering process, where a constant cutoff wavelength of a low-pass Gaussian filter is applied to all samples, smoothing the morphological surface by truncating the peaks and pits. This truncating effect is expected to be more pronounced in the higher spindle speed samples, affecting the trend of  $Sdr$ . Therefore, this trend should only be used as a conclusive result with further investigation.

### Correlation matrix analysis of key variables

This section introduces a correlation matrix analysis encompassing spindle speed, number, and mean of segmented areas,  $Sq$ ,  $Sz$ ,  $Str$ ,  $Sal$ , and  $Sdr$ , as shown in Table 8. The high coefficient values, close to one, indicate a significant correlation between the two parameters [18].

$Sq$  and  $Sz$  are two parameters from the amplitude parameters explaining the two different things based on the morphological surface height. The maximum peak-to-valley height  $Sz$  is very sensitive to the outliers in the surface dataset that may occur due to dirt or measurement errors, while the root mean square height  $Sq$  is stable and less susceptible to outliers. A low-pass filter is applied to reduce the outliers' effect for the current study. However, since the geometrical transcription mainly causes the surface texture formations for the given experimental condition during tool-work interaction, the  $Sz$  and  $Sq$  are becoming interdependent, especially at the range when the spindle speed is less than 3500 rpm, and they are not suitable to be used together to describe the surface. Hence,  $Sq$  is selected between the two.

Table 8: Correlation matrix of segmentation area and roughness parameters

	RPM	Area-Number	Area-Mean	$Sq$	$Sz$	$Sdr$	$Str$	$Sal$
RPM	1.00	1.00	-0.86	-0.97	-0.95	-0.92	0.51	-0.93
Area-Number		1.00	-0.83	-0.96	-0.94	-0.90	0.55	-0.92
Area-Mean			1.00	0.93	0.93	0.98	-0.10	0.95
$Sq$				1.00	0.98	0.98	-0.42	0.99
$Sz$					1.00	0.97	-0.34	0.97
$Sdr$						1.00	-0.24	0.99
$Str$							1.00	-0.37
$Sal$								1.00

A high correlation is also observed between  $Sq$  and the auto-correlation length  $Sal$ . Unlike  $Sq$ ,  $Sal$  is from spatial parameters characterising the spatial information of the surface texture, in this case, the surface prominent wavelength. As explained in Figure 15,  $Sal$  is highly affected by the distance between the surface features but not the surface height. In many cases,  $Sq$  and  $Sal$  are used concurrently to describe a surface [19]. However, in the current study, due to the simple geometrical transcription as in Figure 15, the effect of the surface height on the distance between lays is inevitable, hence explaining the high correlation value between the  $Sq$  and  $Sal$ .

The developed interfacial area ratio  $Sdr$ , on the other hand, despite showing a high correlation with the spindle speeds and other parameters, can only be explained by the effect of the low pass filtering of the measured data, as mentioned in the previous section. Hence, it cannot be used to describe the surface with the current setup and requires further investigation. On the other hand,  $Str$  shows a relatively low correlation with other roughness parameters, as explained in the previous section. Hence,  $Str$  can be used to describe the surface.

Area-mean in Table 8 is the average size of the segmented areas from the trajectory simulation. The area-mean highly correlates to the  $Sq$ ,  $Sz$ ,  $Sdr$ , and  $Sal$ . It shows that the surface roughness can be explained using the trajectory simulation.

## Conclusion

The study successfully employed a mathematical model to simulate a two-flute end mill's tool edge trajectory pattern, mimicking the surface lay pattern in end milling. A visual comparison between experimental and simulated trajectories showcased continuous forward-moving spiral forms. Employing watershed segmentation, simulation outcomes revealed an increase in segmented areas with higher spindle speeds, accompanied by decreased mean



and standard deviation of these regions. Experimental results indicated that increased spindle speed reduced surface roughness metrics ( $Sq$ ,  $Sz$ ,  $Sal$ ), although  $Sdr$  notably diverged from predictions, potentially due to measurement filters. The study's integration of simulation and experimentation underscores the connection between tool trajectories and smoother surfaces in end milling with increased spindle speed. However, this study can only explain the surface texture formation due to simple geometrical transcription during the tool-work interaction at spindle speed between 1000 to 3500 rpm combined with the other fixed machining parameters, while the finer surface roughness formation may need to include other factors such as material behaviours, friction, etc.

## **Contributions of Authors**

The authors confirm the equal contribution in each part of this work. All authors reviewed and approved the final version of this work.

## **Funding**

This work was supported by the Fundamental Research Grant Scheme (Grant no. FRGS/1/018/TK03/UITM/02/13) of the Ministry of Higher Education Malaysia.

## **Conflict of Interests**

All authors declare that they have no conflicts of interest.

## **Acknowledgement**

The authors thank the College of Engineering, Universiti Teknologi MARA, for encouraging this research.

## **References**

- [1] K. Kumar, D. Zindani, and J. P. Davim, "Introduction to Machining Processes," *Advanced Machining and Manufacturing Processes*, Springer International Publishing, Springer International Publishing, 2018, pp. 41-47.

- [2] A. Sharman, D. Aspinwall, R. Dewes, and P. Bowen, "Workpiece surface integrity considerations when finish turning gamma titanium aluminide," *Wear*, vol. 249, no. 5-6, pp. 473-481, 2001. [https://doi.org/10.1016/S0043-1648\(01\)00575-0](https://doi.org/10.1016/S0043-1648(01)00575-0)
- [3] A. M. Zain, H. Haron, and S. Sharif, "Prediction of surface roughness in the end milling machining using Artificial Neural Network," *Expert Systems with Applications*, vol. 37, no. 2, pp. 1755-1768, 2010. <https://doi.org/10.1016/j.eswa.2009.07.033>
- [4] J. G. Parmar and A. Makwana, "Prediction of surface roughness for end milling process using Artificial Neural Network," *International Journal of Modern Engineering Research*, vol. 2, no. 3, pp. 1006-1013, 2012.
- [5] R. Sanjeevi, R. Nagaraja, and B. R. Krishnan, "Vision-based surface roughness accuracy prediction in the CNC milling process (Al6061) using ANN," *Materials Science*, vol. 2214, p. 7853, 2020.
- [6] P. G. Mathews, *Design of Experiments with MINITAB Milwaukee, Wisconsin: ASQ Quality Press*, 2004.
- [7] B. S. Reddy, J. S. Kumar, and K. V. K. Reddy, "Optimization of surface roughness in CNC end milling using response surface methodology and genetic algorithm," *International Journal of Engineering, Science and Technology*, vol. 3, no. 8, pp. 102-109, 2011. <https://doi.org/10.4314/ijest.v3i8.8>
- [8] M. Alauddin, M. El Baradie, and M. Hashmi, "Computer-aided analysis of a surface-roughness model for end milling," *Journal of Materials Processing Technology*, vol. 55, no. 2, pp. 123-127, 1995. [https://doi.org/10.1016/0924-0136\(95\)01795-X](https://doi.org/10.1016/0924-0136(95)01795-X)
- [9] O. Çolak, C. Kurbanoglu, and M. C. Kayacan, "Milling surface roughness prediction using evolutionary programming methods," *Materials & Design*, vol. 28, no. 2, pp. 657-666, 2007. <https://doi.org/10.1016/j.matdes.2005.07.004>
- [10] H. Safari, S. Sharif, S. Izman, and H. Jafari, "High speed dry end milling of Ti-6Al-4V alloy towards nano-scale surface roughness," *Journal of Applied Sciences Research*, vol. 8, no. 11, pp. 5280-5284, 2012.
- [11] P. Benardos and G.-C. Vosniakos, "Predicting surface roughness in machining: a review," *International Journal of Machine Tools and Manufacture*, vol. 43, no. 8, pp. 833-844, 2003.
- [12] D. K. Baek, T. J. Ko, and H. S. Kim, "Optimization of feed rate in a face milling operation using a surface roughness model," *International Journal of Machine Tools and Manufacture*, vol. 41, no. 3, pp. 451-462, 2001. [https://doi.org/10.1016/S0890-6955\(00\)00039-0](https://doi.org/10.1016/S0890-6955(00)00039-0)
- [13] R. Wang, B. Wang, G. C. Barber, J. Gu, and J. D. Schall, "Models for prediction of surface roughness in a face milling process using triangular inserts," *Lubricants*, vol. 7, no. 1, p. 9, 2019. <https://doi.org/10.3390/lubricants7010009>

- [14] Y. Quinsat, L. Sabourin, and C. Lartigue, "Surface topography in ball end milling process: description of a 3D surface roughness parameter," *Journal of Materials Processing Technology*, vol. 195, no. 1-3, pp. 135-143, 2008. <https://doi.org/10.1016/j.jmatprotec.2007.04.129>
- [15] I. Lazoglu, "3D surface topography analysis in 5-axis ball-end milling," *CIRP Annals*, vol. 66, no. 1, pp. 133-136, 2017. <https://doi.org/10.1016/j.cirp.2017.04.021>
- [16] F. Biondani and G. Bissacco, "Effect of cutting edge microgeometry on surface generation in ball end milling," *CIRP annals*, vol. 68, no. 1, pp. 571-574, 2019. <https://doi.org/10.1016/j.cirp.2019.04.017>
- [17] M. Hadad and M. Ramezani, "Modeling and analysis of a novel approach in machining and structuring flat surfaces using face milling process," *International Journal of Machine Tools and Manufacture*, vol. 105, pp. 32-44, 2016. <https://doi.org/10.1016/j.ijmachtools.2016.03.005>
- [18] W. Kirch (eds), "Pearson's Correlation Coefficient", *Encyclopedia of Public Health*, 2008, Springer, Dordrecht. [https://doi.org/10.1007/978-1-4020-5614-7\\_2569](https://doi.org/10.1007/978-1-4020-5614-7_2569)
- [19] P. Pawlus, T. Reizer, M. Wieczorowski, "Functional Importance of Surface Texture Parameters", *Materials*, vol. 14, no. 18, p. 5326, 2021. <https://doi.org/10.3390/ma14185326>